Semicond. Sci. Technol. **15** (2000) 1011–1021. Printed in the UK PII: S0268-1242(00)11445-2

Size-dependent optical edge shifts and electrical conduction behaviour of RF magnetron sputtered CdTe nanocrystals:TiO_2 composite thin films

A C Rastogi, S N Sharma and Sandeep Kohli

Electronic Materials Division, National Physical Laboratory, Dr K S Krishnan Road, New Delhi-110 012, India

Received 31 January 2000, in final form 6 July 2000, accepted for publication 17 August 2000

Abstract. CdTe nanocrystals sequestered and passivated in an amorphous TiO_2 thin film matrix have been prepared by RF sputtering from a composite TiO_2:CdTe target. The CdTe nanocrystal size and volume fraction increases from 15 to 40 nm and 2 to 20% respectively as the film thickness increases, typically from 0.05 to 0.25 μm. A systematic dependence of the optical band edge on the CdTe nanocrystal size shows a strong quantum confinement effect. The optical edge shifts are significantly higher than the theoretical prediction based on single-particle confinement of decoupled electrons and holes. This is understood on the basis of nucleation-controlled growth of CdTe nanocrystals by direct vapour phase condensation, in which small nuclei are rapidly passivated by TiO_2 depositing at much higher rates. The nano-sized CdTe growth island thus formed comprises of several TiO_2 passivated nanocrystals. Electrical conduction behaviour of these films show that tunnelling between the CdTe nanocrystals is not a dominant mechanism, as a three-dimensional network is not realized due to small thickness and lower coverage. The current transport is essentially space-charge-limited. The injection of electrons from nano-sized CdTe crystals follows spherical radial space charge flow which modifies the usual power law dependence from quadratic to 3/2. The analytical description of the current conduction process in composite CdTe:TiO_2 is discussed.

1. Introduction

Nanocrystalline semiconductors are the new class of tunable materials, which exhibit strong size-dependent physio-chemical properties in the size range less than the exciton Bohr diameter of the bulk crystal. Size-dependent chemical reactivity [1,2], optical nonlinearity [3–5], efficient photoelectron emission [6,7] and melting point reduction [8] are some of the interesting properties that have been investigated. These size-tunable properties can be employed for unique applications of these materials. In recent years, nanocrystals of II–VI semiconductors have been the focus of extensive studies on the quantum size effect. These effects are observed when the nanocrystals are isolated in an insulating matrix. CdS [9, 10], CdSe [11–13] and CdTe [13–17] are amongst the most studied cases. CdTe has a large exciton Bohr diameter ∼15 nm, and therefore this semiconductor offers the possibility of studying quantum confinement effects in higher cluster size regimes. The films of CdTe nanocrystalline composites in silicate glass [16], SiO_2 [13], have been prepared using the methods of solution growth [17] and physical vapour deposition (PVD) [15].

Amongst the various PVD techniques, RF sputtering has been the most versatile and proven one. RF sputtering enables the controlled distribution of nanoparticle size and volume over a wide range. In the absence of any thermal processes associated with the technique, no reaction is involved between the matrix and the CdTe nanocrystallites [18]. This technique is also applicable for preparing nanocrystals of many kinds of semiconductor with various absorption edge energies. The thin film structures thus obtained are appropriate for application as devices in sophisticated and complicated systems, such as integrated circuits [13].

In the present study, RF-sputtered CdTe/TiO_2 composite films have been prepared to investigate the quantum confinement effects in CdTe nanocrystals embedded in a TiO_2 matrix. The choice of TiO_2 as a matrix and passivator for CdTe nanocrystals is based on several considerations. TiO_2 is an optically transparent wide bandgap oxide. Thus, the quantum size effects in the optical edge of CdTe nanocrystallites embedded in TiO_2 can be studied over a wide energy range. The electrical resistivity of a TiO_{2-x} film matrix can be varied over a wide range, depending upon the oxygen concentration [19]. This property of TiO_2

0268-1242/00/111011+11$30.00

can be exploited in understanding the electrical conduction mechanism of CdTe nanocrystals dispersed in a TiO_2 matrix for its possible application in devices.

This paper reports the quantum size effects observed in RF-sputtered CdTe:TiO_2 composite thin films of different thicknesses deposited at two substrate temperatures, 27 and 100 °C. Optical absorption spectroscopic studies show that band edge shifts are strongly correlated to crystallite size, indicating strong confinement effects in CdTe nanocrystals passivated by TiO_2. Field-dependent current conduction behaviour of the composite films has been studied to elucidate the effect of the presence of the CdTe nanocrystals. Post-deposition annealing at 400 °C in a H_2/N_2 atmosphere has also been carried out to investigate the effect of oxygen vacancies on the conduction process in CdTe:TiO_2 composite thin films. An analytical description of the current conduction mechanism is discussed.

2. Experimental

The CdTe nanocrystallites embedded in a TiO_2 matrix were prepared by RF magnetron sputtering from a composite target. The target consisted of a TiO_2 sintered disc of 50 mm diameter having a CdTe pellet of diameter 10 mm placed at its centre. Under the typical sputtering conditions, deposition rates of CdTe are about two orders of magnitude higher than that for TiO_2. This makes the growth of CdTe nanocrystals and control of its dispersion in the TiO_2 matrix rather difficult using independent targets. In a composite target, the deposition of CdTe can be substantially reduced by selecting the small-area pellets and by placing them towards the centre of the TiO_2 target, away from the strong sputtering zone. TiO_2 and CdTe were co-sputtered with a RF power of 240–260 W in the presence of Ar gas at 0.02 mbar. The deposition of CdTe:TiO_2 composite thin films was done on quartz substrates held at 27 and 100 °C. Deposition rates of 12–30 Å min^{-1} were used to grow composite films of thicknesses ranging from 500 to 2500 Å. For structural analysis by transmission electron microscopy (TEM), films were deposited on freshly cleaved rock salt crystals. The thicknesses of the films were measured using a quartz crystal thickness monitor. In some cases, post-deposition temperature treatment at 400 °C for 10 min in a H_2/N_2 atmosphere was carried out to investigate the effect of the formation of oxygen vacancies in a TiO_2 film on the conduction process of CdTe:TiO_2 composite thin films.

TEM analysis for the estimation of crystallite size and crystalline phase was carried out using a JEOL electron microscope (JEM-200CX). Optical spectroscopic measurements were carried out in the transmission and reflection mode using a Shimadzu UV-3101 PC spectrophotometer. An identical quartz substrate in the reference beam compensated for any loss in transmission, scattering, etc. in the substrate. Necessary corrections [20] in the measured transmission have been applied for attenuation by reflection at the back side of the substrate and also due to reflections at various interfaces in order to obtain the actual transmittance T_f and reflectance R_f from the film. These parameters can be expressed as [21, 22]

$$T_f = T_{obs}\left(\frac{1 - R'_f R'_s}{1 + R'_s}\right) \tag{1}$$

$$R_f = R_{obs} - \left(\frac{T_f^2 R'_s}{1 - R'_f R'_s}\right) \tag{2}$$

where T_{obs} is the ratio of the measured transmittance of the film–substrate combination to that of the bare substrate and R_{obs} is the ratio of the measured reflectance of the film–substrate combination to that of an aluminium mirror (R_{Al}). R_{Al} was corrected for the optical properties of aluminium so that it can be considered to be unity over the spectral range. R'_f is the backward reflectance from the film side of the film–substrate combination and R'_s is the reflectance at the air–substrate interface for the bare substrate. As R_{obs} was measured by keeping an absorbing surface (a piece of black velvet) at the back, the effect of the back surface and its reflectance was eliminated [20] and R'_f can be regarded as sufficiently close to the measured reflectance R_{obs}. For a non-absorbing substrate (such as quartz), R'_s can be given as

$$R'_s = \frac{(n_s - 1)^2}{(n_s + 1)^2} \tag{3}$$

where n_s is the refractive index of the substrate (for quartz $n_s = 1.44$). The variation of absorption coefficient (α) was calculated from the spectral dependence of the optical reflection (R_f) and transmission (T_f) from Tauc's expression [23].

DC conductivity measurements in the range ($300 < T < 523$ K) were carried out in a vacuum of 10^{-3} Torr. The resistivity in co-planar geometry, using gold film contacts, was measured using a Keithley 617 electrometer. The field dependence of the current was similarly measured using a Keithley 485 picometer.

3. Results and discussion

3.1. Microstructure

Sputter-deposited pure TiO_2 films are amorphous when grown under conditions similar to those employed for the formation of CdTe:TiO_2 composite films. Their surface morphology, whether deposited over substrates held at room temperature (27 °C) or at 100 °C, has a glassy appearance with no discernible structural features. When TiO_2 and CdTe are co-sputtered under similar conditions, CdTe nanocrystals embedded in a glassy TiO_2 matrix are formed.

For very thin 500 Å films, the average CdTe crystal dimensions are ≈11 nm. These crystallites are widely spaced and heterogeneously dispersed. As the film grows thicker with continued sputtering for longer times under similar conditions, the structure becomes different. Although the average CdTe crystal size increases only marginally with film thickness, most importantly a large density of new nanocrystallites is nucleated during prolonged subsequent film growth. Representative microstructures for 500 and 1500 Å thick CdTe:TiO_2 films deposited from the composite target over a substrate held at 27 °C are shown in figures 1(*a*) and (*b*), respectively. The thicker films display a granular

nanostructure where these nanocrystallites are fairly uniform in size and shape and are homogeneously distributed. These nanocrystals have a nearly spherical shape and their morphology appears as circular dots when observed directly by TEM in the direction normal to the film plane. In the early stages of film growth during the co-sputtering process, the CdTe crystallites nucleate at suitable isolated sites within the growing amorphous TiO_2 film. Initially, a sub-nano-sized CdTe crystallite grows essentially by direct condensation and coalescence of additional CdTe molecules from the sputter vapour flux—as lateral diffusion of CdTe in the plane of the film would encounter a higher barrier in the form of TiO_2 molecules also condensing from the vapour phase. It may be noted that, during sputtering, the TiO_2 vapour flux is substantially higher than that of CdTe. The CdTe crystallites are thus expected to grow completely surrounded by TiO_2, yielding spherical shapes. This ensures full passivation of the surface of the CdTe nanocrystals. This growth mode is supported by the observation that, with increase in film thickness, there is an increase in the density of CdTe crystallites without much increase in their crystal size. As the sputter deposition continues for the growth of thicker films, the passivated CdTe nanocrystals inhibit condensation and attachment of additional CdTe molecules from the vapour phase. Thus, with increase in sputtering time, new CdTe crystals are nucleated at different locations within the bulk of the growing TiO_2 films, in preference to the growth in size of the already nucleated ones.

The growth of CdTe crystallites by lateral migration of ad-atoms can be increased by sputter deposition at elevated substrate temperatures. Figure 2(*a*) shows the microstructure of a 500 Å thin film deposited under identical conditions but at a substrate temperature of 100 °C. Although a large number of spherical crystallites are still formed, a number of them show an oblong shape. These features are characteristic of two or more coalescing spherical crystallites. The nucleation density of CdTe crystals has also increased in comparison to the film deposited at 27 °C. The volume fraction of CdTe crystallite has been estimated from the TEM analysis. For a 500 Å thick film grown on a substrate held at room temperature, the CdTe volume fraction has increased from a mere 2 to ∼20% by depositing on a substrate held at 100 °C. The CdTe volume fraction increases in the same proportion as the film thickness for room-temperature-deposited films. For a 1500 Å thick film the CdTe volume fraction increases to 6.5%.

The select area electron diffraction (SAD) studies were carried out to understand the CdTe crystallite structure. The results are shown in the inset of figures 1(*a*), (*b*) and 2(*a*). At low film thickness, due to sparse CdTe crystallites, the diffraction pattern is a broad halo showing an amorphous-like structure, essentially belonging to the TiO_2 matrix. At a higher 1500 Å film thickness, the diffraction pattern is like a smeared ring due to some increase in the volume fraction of CdTe crystallites, although the crystal size is still very small. Growth of CdTe nanocrystals at an elevated temperature yields better crystallite structure as inferred from the ring pattern superimposed by diffraction spots for a 500 Å thin film (figure 2(*a*)). The diffraction pattern from a thicker 1500 Å film deposited at 100 °C, having a much larger CdTe

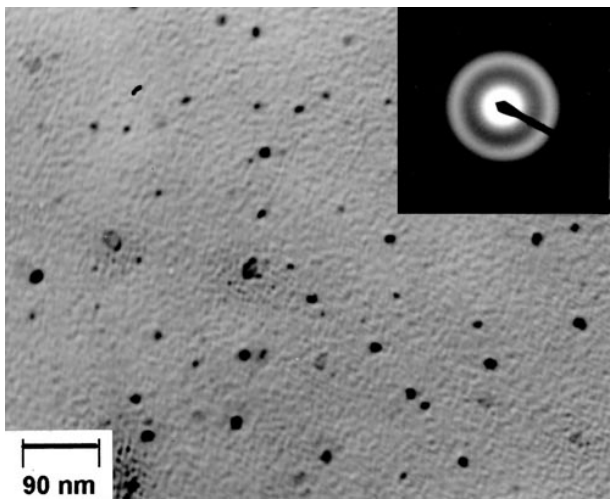

(*a*)

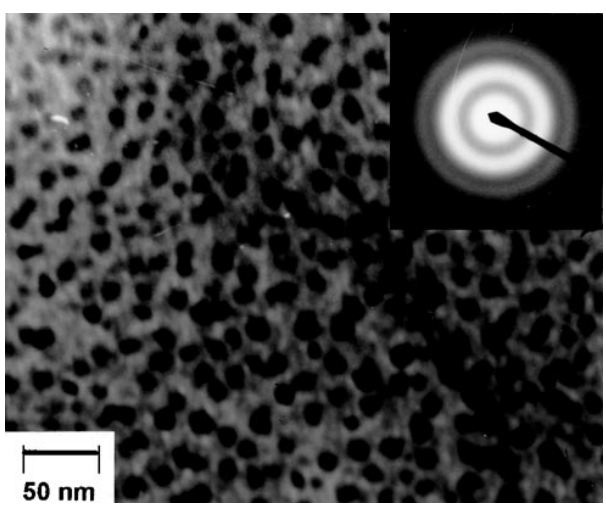

(*b*)

Figure 1. Transmission electron micrograph (TEM) of CdTe nanocrystals dispersed in a TiO_2 thin film matrix for films of thickness (*a*) 500 Å (*b*) 1500 Å deposited at $T_s = 27$ °C. Insets show the selected area diffraction pattern for the corresponding samples.

volume fraction, is shown in figure 2(*b*). Interpretation of the diffraction pattern reveals that the CdTe crystallite grows in a hexagonal wurtzite structure. It may be noted that a pure CdTe film deposited by sputtering shows predominantly a cubic zinc blende structure.

3.2. Optical absorption

Absorbance of the TiO_2 films with CdTe nanocrystallite dispersions depends both on the nanocrystallite size and volume fraction. Figures 3 and 4 show absorption spectra of CdTe:TiO_2 films of different thickness deposited at 27 and 100 °C, respectively, which represent films having different sizes of CdTe nanocrystals and their volume fractions. The absorption curve (d) for a sputter-deposited polycrystalline 3100 Å thick CdTe film displaying a high absorption coefficient is also shown. CdTe nanocrystals in a TiO_2 film, on the other hand, show a much lower absorption coefficient. The optical absorption coefficient gradually

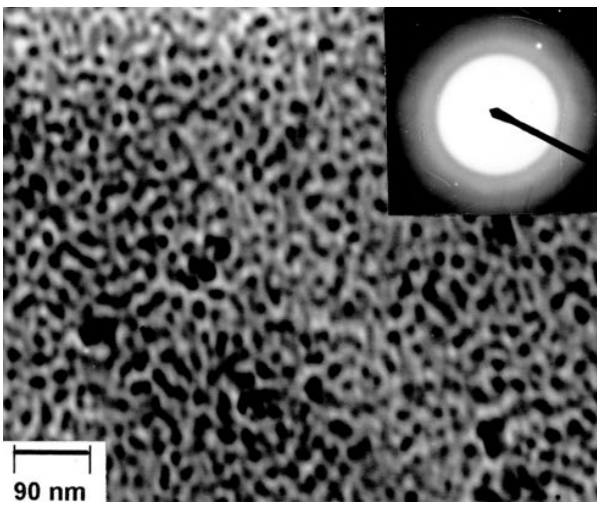

(*a*)

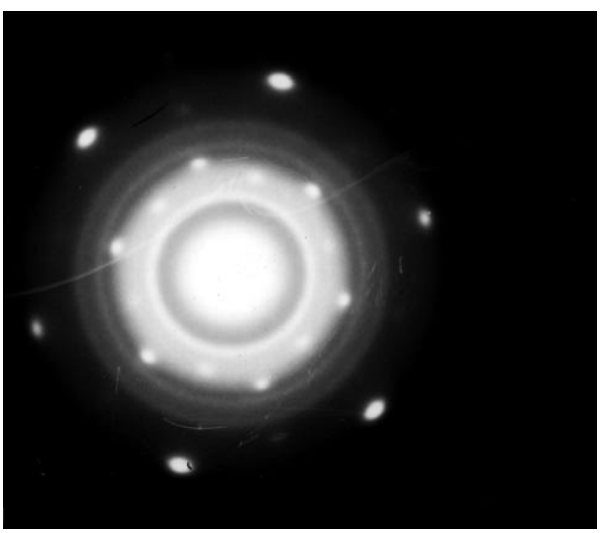

(*b*)

Figure 2. (*a*) TEM of CdTe nanocrystals dispersed in a TiO_2 matrix for a film of thickness 500 Å deposited at $T_s = 100\,^{\circ}C$. (*b*) Selected area diffraction pattern for a 1500 Å thick film deposited at $T_s = 100\,^{\circ}C$.

increases with the increase in thickness of the film due to increased volume fraction of CdTe crystallites within the amorphous TiO_2 matrix. This is accompanied by a gradual shift in absorption edge to the longer wavelength side (red shift) due to the increase in the CdTe nanocrystal size with film thickness. The CdTe polycrystalline film shows a well-defined absorption edge. The direct parabolic band–band transition energies have been measured to compare the shifts due to nano-sized crystallites in TiO_2. The absorption edge for a CdTe:TiO_2 composite film has been estimated from the numerical first derivative of the absorption spectra in the relevant wavelength region. This is shown in figure 5 for the CdTe nanocrystal films deposited at a substrate temperature of 100 °C. The energy at which deviation from a minimum value begins provides an indication of the fundamental absorption edge [24]. For a 3100 Å sputter-coated pure CdTe film, the band edge determined from this technique is 1.54 eV, which is quite close to a number of reported values for CdTe films [25]. The absorption edge shifts to the higher energy

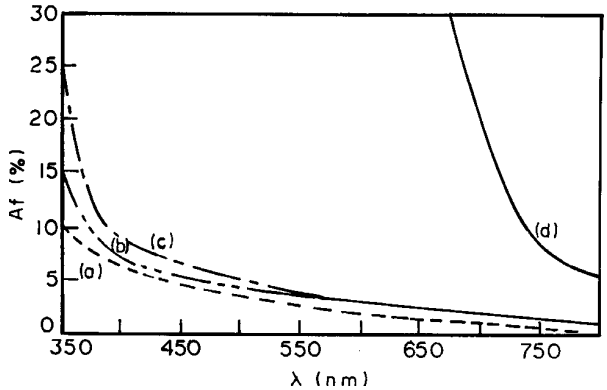

Figure 3. Absorption spectra for CdTe:TiO_2 films of thickness (a) 500 Å, (b) 1500 Å and (c) 2500 Å deposited at $T_s = 27\,^{\circ}C$. (d) Absorption spectra of a polycrystalline CdTe thin film.

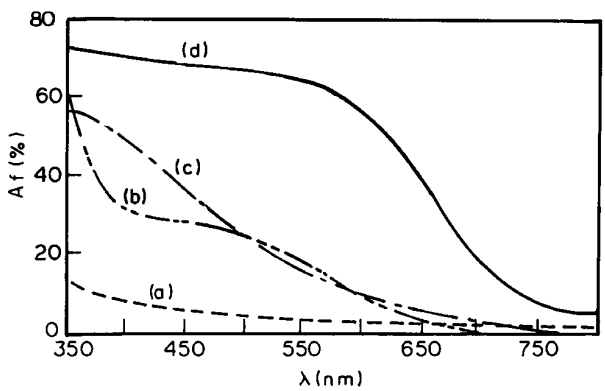

Figure 4. Absorption spectra for the CdTe:TiO_2 films of thickness (a) 500 Å, (b) 1500 Å and (c) 2500 Å deposited at $T_s = 100\,^{\circ}C$. (d) Absorption spectra of a polycrystalline CdTe thin film.

side (blue shift) when CdTe nanocrystals are formed in TiO_2 films. For a very thin 500 Å film the absorption edge occurs at ∼2.16 eV.

The shift $\Delta E_g = (E_g$ (nanocrystal CdTe)–E_g (polycrystalline CdTe)) is largest (0.62 eV) for very thin (500 Å) films. The band edge shift reduces as the film thickness increases, due to a corresponding increase in CdTe nanocrystal dimensions. For 1500 and 2500 Å films, the band edge shift is 0.29 and 0.16 eV, respectively. For room-temperature-deposited films, there is no discernible change in slope of the differential absorption spectra, making the location of the absorption edge difficult. These films have a very small density of CdTe dispersions. Due to low absorption from the CdTe nanocrystals, the absorption spectra are heavily modulated by features of the TiO_2 band to band transition and band tailing effect.

The optical absorption data are well correlated with the microstructure features and crystalline phase of CdTe nanocrystals sequestered in TiO_2 films. The blue shifts in the band edge from bulk CdTe values with the reduction in crystal size are attributed to the effects of quantum confinement on the electronic band structure of CdTe. The quantum size effects in thin films of CdTe nanocrystallites in a glass matrix [16] and SiO_2 have been reported earlier. The quantum effect becomes apparent when the semiconductor crystal size is smaller than the bulk Bohr radius of the

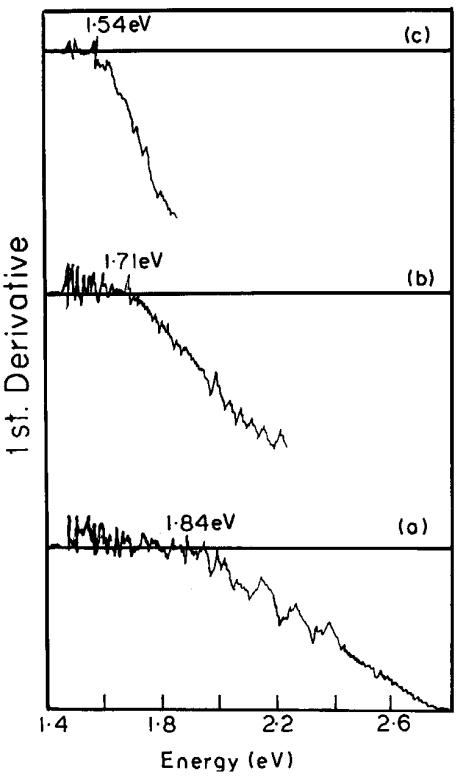

Figure 5. Numerical first derivative of the absorption spectra for CdTe:TiO_2 composite films of thickness (a) 1500 Å and (b) 2500 Å deposited at $T_s = 100\,^{\circ}$C. Curve (c) is for a polycrystalline CdTe thin film.

Wannier exciton R_B. For CdTe, this value is ∼15 nm [15]. In the present study for most of the TiO_2:CdTe composite films, the average CdTe nanocrystal size is ∼11–15 nm. Quantum confinement of an electron–hole pair in the infinite spherical potential well is represented by a CdTe spherical crystallite bound by a high band gap TiO_2. The effect of band structure on optical absorption edge shifts due to the quantum size effect is described theoretically on the basis of two confinement regimes [26] depending on whether the nanocrystallite size (R_{nc}) to Bohr exciton diameter (R_B) ratios (R_{nc}/R_B) are $\ll 2$ or $\geqslant 4$. The former case represents strong confinement, in which electrons and holes are independently confined when the CdTe nanocrystals (average radius r_{nc}) are much smaller than R_B. The exciton energy on the size of nanocrystals is given by

$$E(R) = E_{bulk}(\mathrm{CdTe}) + \frac{2\hbar^2}{\mu}\left(\frac{\pi}{R_{nc}}\right)^2 \qquad (4)$$

where μ is the effective mass of an electron–hole pair given by

$$\frac{1}{\mu} = \frac{1}{m_e} + \frac{1}{m_h}.$$

In the weak confinement regime, when the CdTe nanocrystal size is greater than $4R_B$ the exciton within the nanocrystals show translational motion confinement due to strong Coulomb interaction. The excitonic energy is given by the above relation, except that the effective mass of the electron–hole (μ) is replaced by the total mass of the exciton $M = m_e + m_h$ and is represented by

$$E(R) = E_{bulk}(\mathrm{CdTe}) + \frac{2\hbar^2}{M}\left(\frac{\pi}{R_{nc}}\right)^2. \qquad (5)$$

In both cases of quantum confinement, the excitonic shift in the energy change scales linearly with the inverse square of the CdTe nanocrystal size ($1/R_{nc}^2$), where R_{nc} is the average size of the CdTe crystallites. The theoretical dependence of the transition energy on the two extreme confinement situations on the inverse squared average CdTe crystal size has been analysed in figure 6. The translational reduced mass of the exciton is taken as $M = 0.5m_0$ and the exciton reduced mass as $\mu = 0.08m_0$, where m_0 is the rest mass of the electron [27]. The bulk Bohr diameter of the Wannier exciton in CdTe is ∼15 nm. Except in the case of a 500 Å thin film, where the average size of the CdTe nanocrystal to Bohr diameter ratio is close to 1, in most other films this falls between 1 and 2.6. Thus, threshold absorption edge shift should show the effect of single-particle confinement. However, the value of the absorption edge derived from the absorption data is much higher than that calculated theoretically from excitonic confinement. The disagreement of our experimental results could be attributed to a number of factors arising from poor crystallinity of CdTe and distribution in their shape, which may result in inhomogeneous broadening of quantum confined states. There is neither any evidence of reaction between the TiO_2 matrix and CdTe nor, as our electron diffraction analysis shows, is there any composition change in CdTe, which may affect the CdTe nanocrystal band structure. The most probable cause of large shifts in band edges can be understood on the basis of the anisotropic nature of the sputter deposition of CdTe crystallites in TiO_2. As discussed earlier, the CdTe crystallites grow at isolated nucleation sites and are concurrently passivated by a high rate of condensing TiO_2 vapour flux. Thus, a typical nano-sized CdTe growth island as observed by TEM could, in fact, be a cluster of several smaller nanocrystals, each surrounded and surface passivated by TiO_2. Figure 7 shows a TEM micrograph taken at a higher magnification where, in a few 15 nm sized CdTe growth islands, clustering of several smaller nanocrystallites of CdTe could be seen. The broken line in figure 6 correlates the size of nanocrystals determined experimentally and that expected on the basis of the strong confinement regime. This yields a discrepancy in size typically of a factor of 3 times for larger crystallites and 2.6 times for smaller ones. With 50% packing fraction of smaller nanocrystals within a CdTe growth island there may be about 8–15 smaller nanocrystals.

3.3. Electrical conduction

Detailed knowledge of the conduction behaviour of CdTe nanocrystals is important for devices. The sputtered TiO_2 films forming the matrix for CdTe nanocrystals are amorphous. In a three-dimensional network, the electrons would have to overcome the energy barrier at the CdTe nanocrystal–TiO_2 interface in order to transfer from CdTe nanocrystals and conduct across the TiO_2 matrix for

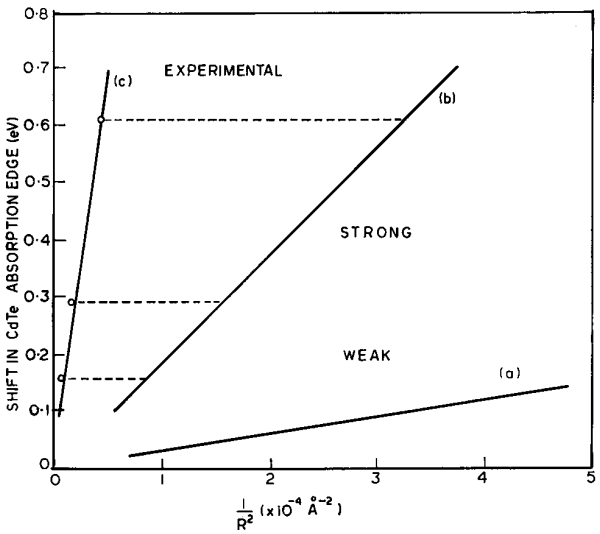

Figure 6. Theoretical blue shifts in the CdTe absorption edge as a function of inverse squared average CdTe crystal size corresponding to (a) translational exciton mass (weak confinement) and (b) exciton reduced mass (strong confinement). Experimentally observed blue shifts for different samples with different nanocrystalline sizes as measured from TEM analysis are shown as curve (c).

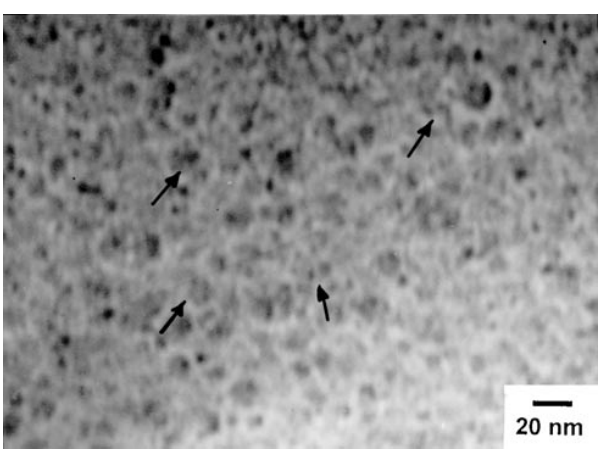

Figure 7. TEM showing the clustering of several smaller sized CdTe nanocrystals, more clearly shown in a few CdTe growth islands marked by arrows. The islands have an average size ∼15 nm and are dispersed in the TiO_2 matrix for a 1500 Å thick film deposited at $T_s = 27\,^{\circ}$C.

collection at the electrode. The temperature dependence of the electrical conductivity of TiO_2 films having different volume fractions of CdTe nanocrystals was studied at a constant field of 0.4×10^3 V cm^{-1}. The results are shown as Arrhenius plots $\ln\sigma$ versus T^{-1} in figure 8. It is seen that conductivity decreases with increase in CdTe volume fraction and film thickness. These plots show a reasonable straight-line behaviour above room temperature. The slopes of the conductivity plots decrease with the increase in the film thickness, which corresponds to an increase in CdTe nanocrystal volume fraction. The DC activation energy values derived for carriers are 0.83, 0.74 and 0.63 eV, for CdTe:TiO_2 films of thicknesses 500, 1500 and 2500 Å, respectively. The conductivity of CdTe:TiO_2 films decreases with increase in CdTe volume fraction and the film thickness.

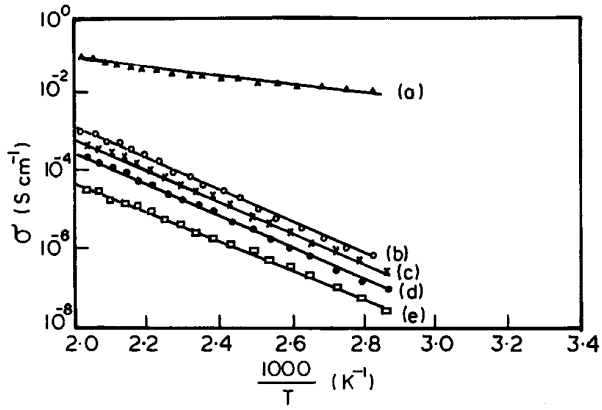

Figure 8. Temperature-dependent DC conductivity of (a) polycrystalline CdTe thin film and CdTe:TiO_2 composite films of thickness (b) 500 Å, (c) 1500 Å, (d) 2500 Å and (e) pure TiO_2 film of thickness 2500 Å.

This observation is different from an earlier study by Fuji *et al* [28] on thin films of Ge nanocrystals embedded in a SiO_2 matrix, which reported an increase in room-temperature conductivity by more than 3 orders of magnitude as the Ge nanocrystal volume fraction in the films is increased from 4.2 to 15.3%. This has been attributed to the formation of a Ge nanocrystal network, in which the thermally activated electron tunnelling between the nanocrystals dominates the conduction process. Using the concept developed earlier for metal dispersions in insulators [29, 30], the linear dependence of $\ln\sigma$ versus $T^{-1/2}$ observed by these authors has been interpreted as due to activated tunnelling between neighbouring particles where the activation energy is taken as the electrostatic charging energy of a particle for tunnelling. Our conductivity data do not follow the linear $T^{-1/2}$ dependence, suggesting that the activation energy derived from plots in figure 8 could not be attributed to the electrostatic energy required for transfer of an electron from one nanocrystal of CdTe to another. Clearly, thermally assisted tunnelling between the CdTe nanocrystallites does not appear to be a dominant conduction process. Further, as the volume fraction of CdTe as well as film thickness is increased, the room-temperature conductivity, instead of increasing, showed a decrease, which indicates that there is no formation of a CdTe nanocrystal network. With the increase in CdTe volume fraction and decrease in inter-crystallite spacing, the increase in conductivity should be expected on this basis. The conduction process in the CdTe:TiO_2 films appears to be dominated by the TiO_2 matrix. Conduction in TiO_2 films is due to oxygen vacancies which act as donors. We have carried out hydrogen annealing studies in order to create oxygen vacancies and increase the conductivity. Figure 9 shows the $\ln\sigma$ versus T^{-1} plot of CdTe:TiO_2 films of thicknesses 500 and 1500 Å after annealing at 400 °C in hydrogen ambient for 10 min each. The room-temperature conductivity of the two films increased by five times after annealing. This increase was similar to that observed for pure TiO_2 films without the CdTe nanocrystals.

We have investigated the electric field (E) dependent current (J) transport behaviour of these films at different

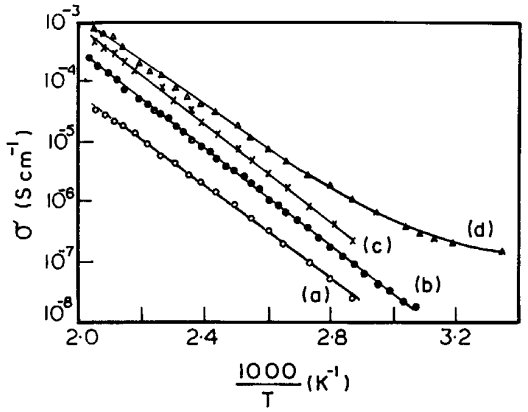

Figure 9. Temperature dependence of DC conductivity of CdTe:TiO_2 films before and after the hydrogen annealing treatment. Curves (a) and (c) are for as-deposited 1500 and 500 Å thick films, respectively, and curves (b) and (d) are for the corresponding films after annealing in hydrogen ambient at 400 °C for 10 min.

temperatures. Typical results of this study are shown as $\log J$ versus $\log E$ plots in figures 10(*a*) and (*b*) and 11(*a*) and (*b*) for CdTe:TiO_2 composite and pure TiO_2 thin films, respectively. In both cases, the current follows a power law dependence, $J \propto V^m$, over a wide range of current extending over three orders of magnitude and over two decades in voltage. The value of the exponent m shows a distinct behaviour for CdTe:TiO_2 and TiO_2 films. As seen in figure 10(*a*) for a (1500 Å) thick CdTe:TiO_2 film having CdTe nanocrystals of average size ∼12.5 nm in volume fraction of ∼6.5%, the exponent m has a value of ∼1.5 over a range of fields 3×10^3–3×10^4 V cm^{-1} at 140 °C. At still higher temperatures 188 and 240 °C in the high field regime, the value of the exponent m changes to 2.0 and 2.3, respectively, although at low fields at 240 °C, it still has a value of ∼1.45 which is close to 1.5. This behaviour was consistently seen over a number of identically prepared CdTe:TiO_2 composite films. Figure 10(*b*) shows $\log J$ versus $\log E$ data for another CdTe:TiO_2 film of thickness 2500 Å, which shows a similar dependence of m over different applied fields. In fact, in several CdTe:TiO_2 composite films, the value of the exponent m was consistently equal to 1.5 ± 0.05. For pure TiO_2 films both the value of the exponent m, as well as the nature of the field dependence, is considerably different. As shown in figure 11(*a*), at lower applied fields, the current follows a linear dependence ($J \propto V$) with $m \sim 1$, which deviates at higher fields into a power law behaviour. The current follows a quadratic behaviour with $m \cong 2$ at higher fields at higher temperatures. For a 2500 Å thick TiO_2 film, figure 11(*a*), the m value is 1.9, 2.0 and 2.1 in the high field $>2.3 \times 10^3$ V cm^{-1} region, depending upon the measurement temperature. Figure 11(*b*) shows the typical data for a thicker (5000 Å) TiO_2 film. The value of m at higher fields is typically 1.88, 1.80 and 2.1, depending on the temperature. In fact, consistent data over a number of TiO_2 films studied yields $m = 1.0 \pm 0.15$ at lower fields and $m = 2 \pm 0.2$ at higher fields.

The origin of the power law dependence is ascribed to the existence of space charge limited (SCL) currents. It is seen that the field at which the deviation from linear

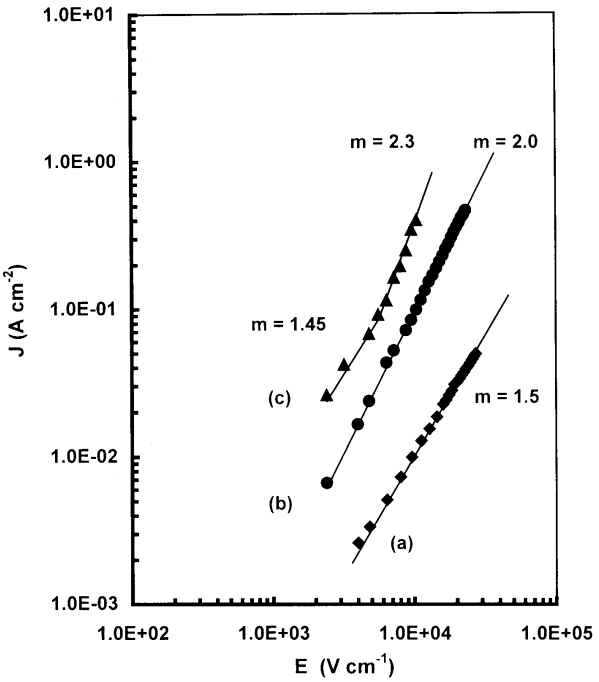

(*a*)

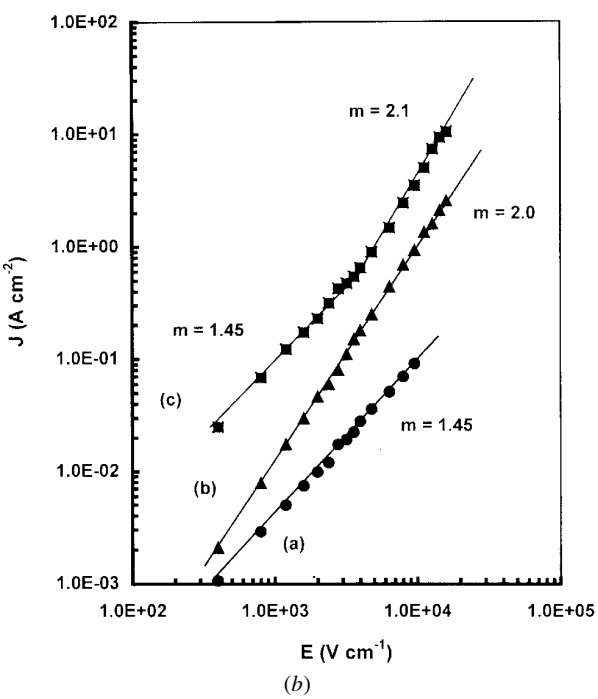

(*b*)

Figure 10. (a) Log–log plots of current density (J) with electric field (E) for the room-temperature-deposited 1500 Å thick CdTe:TiO_2 film measured at different temperatures, (a) 140 °C, (b) 188 °C and (c) 240 °C. (b) Log–log plots of current density (J) with electric field (E) for the room-temperature-deposited 2500 Å thick CdTe:TiO_2 film measured at different temperatures, (a) 140 °C, (b) 188 °C and (c) 240 °C.

Ohm's law behaviour takes place shifts to higher values as the measurement temperature is increased. This is due to the increase in thermal carrier densities and, to sustain the space charge, a higher free electron injection is required. In pure TiO_2 films without the CdTe nanocrystals, the current

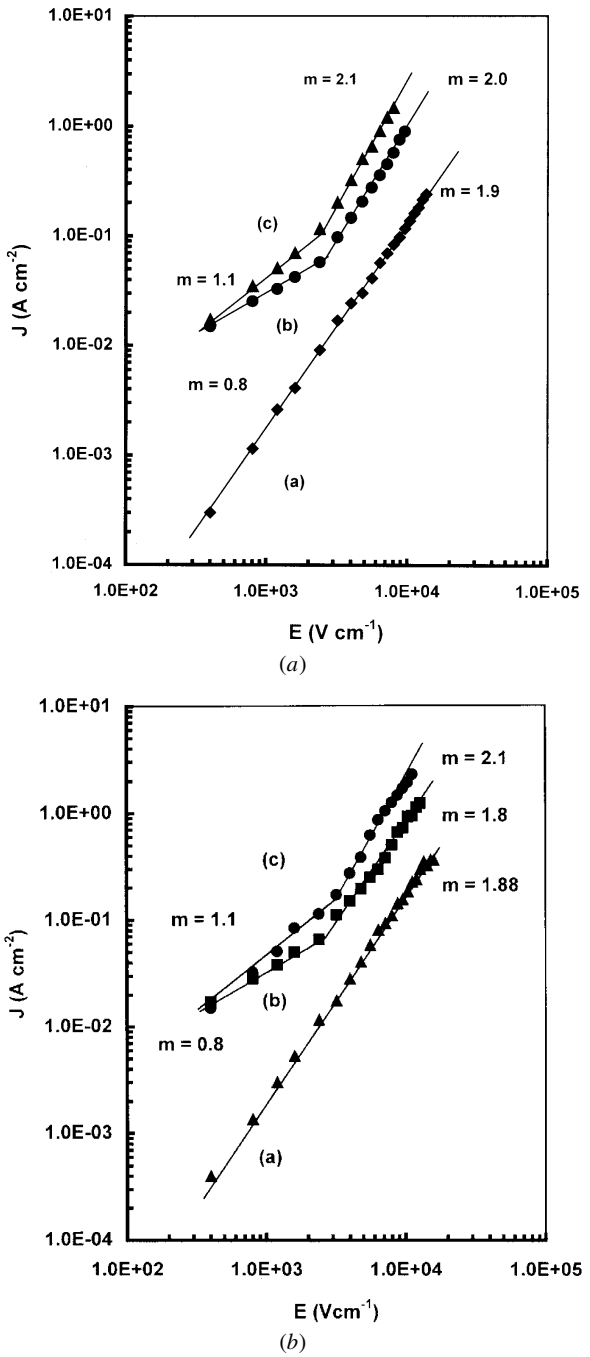

Figure 11. (*a*) Log–log plots of current density (J) with electric field (E) for the room-temperature-deposited 2500 Å thick pure TiO_2 film measured at different temperatures, (a) 140 °C, (b) 188 °C and (c) 240 °C. (*b*) Log–log plots of current density (J) with electric field (E) for the room-temperature-deposited 5000 Å thick pure TiO_2 film measured at (a) 140 °C, (b) 188 °C and (c) 240 °C.

transport is dominated by SCL current flow. As shown by Lampart and Mark [31], the SCL current is given by

$$I = \theta \varepsilon_i \mu [V^2/d^3] \tag{6}$$

where ε_i is the static dielectric constant of a TiO_2 insulator. The factor θ is the ratio of total (equilibrium and injected) concentration of free carriers to those trapped by defect states (n_t). The free carrier density present in TiO_2 is given by

$$n_0 = N_c \exp\left(\frac{-(E_c - E_f)}{kT}\right) \tag{7}$$

where N_c is the effective density of state and E_f is the Fermi level. Accordingly, θ is expressed as

$$\theta = \frac{n_0}{n_t} = \frac{N_c}{N_t} \exp\left(\frac{-(E_c - E_f)}{kT}\right). \tag{8}$$

The quadratic ($I \propto V^2$) power law behaviour is observed experimentally as shown in figure 11. The departure from the linear ohmic law at lower fields implies that the injected carriers are comparable to or exceed the thermally generated free carriers n_0. Thus, at 140 °C, V^2 dependence is observed even at fields as low as 1.4×10^3 V cm^{-1}. As the temperature rises, a corresponding increase in thermally generated carriers ensures ohmic behaviour, even at higher fields as seen in curves (b) and (c) of figure 11. The total trapped space charge per unit area, which has to be supported for SCL flow, is given by qN_td. The transition from initial ohmic behaviour to quadratic SCL conduction occurs at a transition voltage V_x which is expressed as

$$V_x = \frac{qN_td^2}{\varepsilon_i \varepsilon_0}. \tag{9}$$

Assuming carrier mobility $\mu \sim 0.1$ cm^2 V^{-1} s^{-1}, θ values were determined at various temperatures from the intercept of the power law dependence given by equation (6). The dominant trap state governing the SCL current flow is found at 1.6 eV below the conduction band. This is obtained by exponential dependence of θ with T as given by equation (8). The trap state is near the mid-gap region and lies much below the Fermi level. The total density of the trap state is given by equation (9). Using relevant parameters its characteristic value is determined as $\sim 5 \times 10^{12}$ cm^{-3}.

3.4. Theoretical analysis

The current transport in this system, where CdTe semiconductor nanocrystal particles are sequestered in an amorphous insulator (TiO_2) matrix, has been analysed in terms of (i) injection of carriers at the external metal (Au)–TiO_2 contact and (ii) injection of carriers from the CdTe semiconductor nanocrystals into the TiO_2 matrix. In the former case, the injected electrons, under the influence of an applied electric field, drift across the contacts, suffer frequent collisions with thermal phonons, impurities or get trapped/detrapped at the defects. This injection of carriers across the ohmic contacts is facilitated by bending of the bands. In the case of a CdTe:TiO_2 interface as encountered within the composite film, almost all the band bending occurs in the TiO_2. The electron concentration within the CdTe remains undisturbed. The injection occurs from the CdTe region into TiO_2 as the energy bands narrow by an increase in field. This is shown by a schematic of the energy band diagram in figure 12(*a*) where CdTe nanocrystals are separated by wide gap ($E_g \sim 3.5$ eV) TiO_2 barriers. The nano-sized CdTe crystallites show a size-dependent band gap,

$E_{g4} > E_{g3} > E_{g2} > E_{g1}$ which is greater than its bulk value, due to quantum confinement effects. The band connectivity between the CdTe semiconductor and the TiO_2 insulator is tentative, as band offset between conduction and valence bands of CdTe and TiO_2 has not been taken into account. The current flow in the case of carrier injection from the large area Au electrodes across the film plane is planar. This is different from the flow of carriers that takes place from an isolated nano region of the CdTe semiconductor into TiO_2 which spreads around the CdTe nanocrystal in a spherical geometry into the TiO_2. Thus, in TiO_2:CdTe nanocrystal composite films, the analytical problem of injection from the CdTe semiconductor nanocrystals involves a radial flow of current from a spherical geometry into the region of TiO_2 surrounding the nanocrystal (see schematic figure 12(*b*)). The way the charge is injected in the immediate vicinity of the CdTe nanocrystal spreads with the applied field determines the power law dependence (the m parameter). At low fields, the carriers follow the ohmic dependence if the carriers are confined in a radius (r) less than the diameter of the CdTe nanocrystal ($r < 2r_{nc}$). As the field is increased, the carriers are pushed out into the TiO_2 matrix region. As the carriers injected from CdTe nanocrystal decrease monotonically in spherical geometry around it, one can define an arbitrary spherical boundary of radius r_0 below which the injected charge n_i exceeds the free carriers n_0 present in TiO_2 (region I) and above which the thermal free carriers n_0 exceed the injected carriers (region II). One can thus neglect n_0 in region I and n_i in region II. In region I, where $r_{nc} \leqslant r \leqslant r_0$, the injection current flowing in spherical geometry is given by the particle conservation equation:

$$I = 4\pi e\mu n_i r^2 E \tag{10}$$

where E is the electric field and n_i is the injected charge from the CdTe nanocrystals over the thermal carriers n_0 already present such that $n_i = n - n_0$. n_i will decrease monotonically at a distance r from r_{nc}. Beyond this region, i.e. in region II where $r_0 \leqslant r \leqslant r_i$ where r_i represents a region of TiO_2 insulator much farther from the injected CdTe nanocrystal,

$$I = 4\pi e\mu n_0 r^2 E. \tag{11}$$

An externally applied voltage V is distributed across the two regions:

$$V = V_{nc,0} + V_{0,i}$$
$$V_{nc,0} = \int_{r_{nc}}^{r_0} E\,\mathrm{d}r, \qquad V_{0,i} = \int_{r_0}^{r_i} E\,\mathrm{d}r. \tag{12}$$

In region I, the voltage is given by

$$V_{nc,0} = k_1 E_0 r_0.$$

As at the r_0 boundary of region I, $n_i = n_0$ and $n_{t,i} = n_{t,0}$, where $n_{t,i}$ is the average injected excess trap electrons and $n_{t,0}$ the trap electrons in equilibrium with free electrons. The total charge in region I is expressed as [31]

$$Q_0 = \frac{4\pi}{3} r_0^3 (n_0 + n_{t,0}). \tag{13}$$

This charge is presumed to be uniformly distributed over the region I.

Similarly in the ohmic region II

$$V = V_{0,i} = E_0 \cdot r_0.$$

Integrating equation (12) within limits one gets

$$V = (1 + k) r_0 E_0. \tag{14}$$

The ohmic current term of region II (equation (11)) is modified as

$$I = 4\pi e\mu n_0 r_0 V/(1 + k).$$

One can write Poisson's equation in spherical geometry in the region around the CdTe nanocrystal as

$$\frac{\mathrm{d}}{\mathrm{d}r}(r^2 E) = \frac{Q}{4\pi\varepsilon}.$$

Integrating the differential within the limits r_{nc}, r_0:

$$r_0^2 E_0 = \frac{Q_0}{4\pi\varepsilon}. \tag{15}$$

Inserting the value of Q_0 and E_0 from equations (13) and (14), respectively, in the above equation (15), we get

$$r_0 = \left(\frac{3\varepsilon V}{e(n_0 + n_{t,0})}\right)^{1/2}. \tag{16}$$

Substituting this into equation (11), the expression for the current through the TiO_2 matrix in the presence of a CdTe nanocrystal is given by

$$I = 4\pi n_0 \mu \left(\frac{3\varepsilon e}{(n_0 + n_{t,0})}\right)^{1/2} \cdot V^{3/2}. \tag{17}$$

The power law dependence $I \propto V^{3/2}$ has been experimentally observed as seen in curves (a) in figures 10(*a*) and (*b*). The linear behaviour of current at low fields is not observed due to the low density of free carriers in highly resistive films. At a higher measurement temperature of 188 °C, the usual 3/2 power law behaviour disappears and the characteristic quadratic law characteristic of a planar carrier transport through the insulating TiO_2 is seen. With increase in temperature, the possibility of a higher number of free carriers also increases. Activated temperature dependence of conduction (see figure 8) arises from the minimum energy for a carrier to be thermally emitted into the band from a trap state or across the band edge. As a consequence, the region $r_{nc} \leqslant r \leqslant r_0$ shrinks with the reduction in r_0 values (see equation (16)) and the analytical problem of conduction reduces to that of planar flow across a TiO_2 matrix. At a still higher temperature ~240 °C the concurrent appearance of 3/2 and square law behaviour is observed, see figures 10(*a*) and (*b*). Here, one observes $m = 1.45$ (close to the 3/2 power law) at low fields and $m = 2.3$ and 2.1 (close to the quadratic power law) at higher fields. This is attributed to the difference in the injection of carriers from the two regions I and II on applied field. Increase in field also corresponds to an increase in charge density in the CdTe:TiO_2 composite film. With the increase in the current, the region around the CdTe nanocrystals which is responsible for the 3/2 power law dependence increases as 1/3 power of the injection level current. On the other hand, the planar flow from injection from

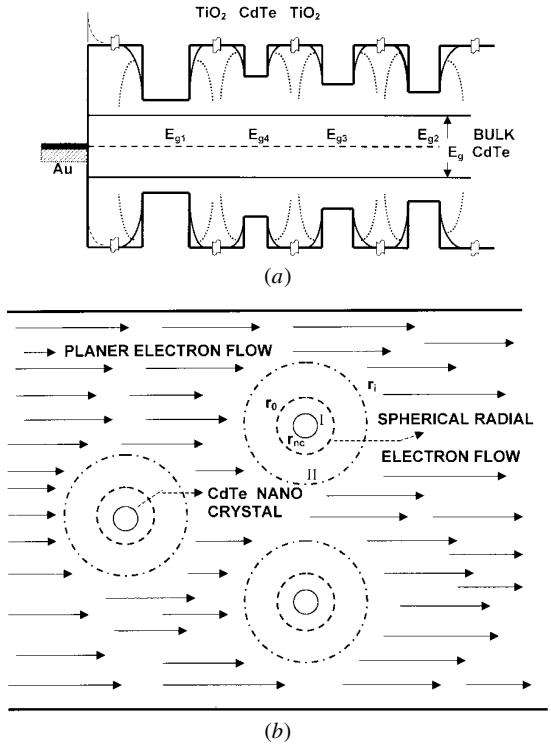

Figure 12. (*a*) Schematic energy band diagram of CdTe nanocrystal quantum dots shown by dotted lines separated by wide gap ($E_g \sim 3.5$ eV) TiO_2 barriers. The energy gap of CdTe varies with nanocrystal size. The break in the conduction band of TiO_2 indicates a difference in dimensions of the TiO_2 region and CdTe nanocrystals. Injection occurs from the CdTe region into TiO_2 as the energy bands narrow by an increase in the field. (*b*) Radial flow of current from the spherical CdTe nanocrystals into the surrounding TiO_2 region and planar flow of current in extended TiO_2 regions.

electrodes into the CdTe:TiO_2 film is linear [31]. Since the region boundary in tthe spherical case of carrier injection from a CdTe nanocrystal into TiO_2 moves slowly with current (or applied field), one can observe both power law dependences in specific field regimes. As can be seen from figures 10(*a*) and (*b*) curves (c), such a situation indeed exist in the current-field plots. At other temperatures, for observing the $m = 1.5$ and 2.0 behaviour, the field regions may be different from those experimentally measured in the present study.

4. Conclusions

Using RF sputtering from a composite CdTe:TiO_2 target, fully passivated CdTe nanocrystals without any compositional variation and reaction with TiO_2 matrix were realized. Systematic optical band edge shifts and microstructural data show strong quantum confinement. Significant deviation from the theoretically predicted band edge shifts on crystal size for strong decoupled electron and hole single-particle confinement behaviour is understood on the basis of the formation of clusters of several smaller nano-sized and TiO_2 passivated CdTe crystallites within a CdTe growth island. The other purpose of this study was to be able to alter the conductivity of the system through O_2^- vacancies and investigate the effects of electrostatic charging of nanocrystals. The effect of oxygen vacancies on the expected conductivity changes were not observed as the film thicknesses were too small to form a three-dimensional network of CdTe nanocrystals. Conduction is not due to thermally assisted tunnelling of carriers between the adjacent CdTe nanocrystals. The current transport in these films is due to the SCL mechanism. The injection of carriers from a CdTe nanocrystal follows the spherical radial flow into TiO_2. This modifies the more dominant planar SCL current transport through the TiO_2 insulating matrix under certain conditions of field and temperature to yield a $3/2$ power law dependence instead of the usual quadratic flow.

Acknowledgments

We thank the Director, National Physical Laboratory for permission to publish this research. Acknowledgments are also due to the Electron Microscopy Group for help in TEM studies and Dr (Mrs) M Kar for optical measurements. We also thank the Ministry of Non-Conventional Energy Sources (MNES) for the financial support through a sponsored project on development of CdTe solar cells. SK acknowledges the research associateship awarded by the Council of Scientific and Industrial Research (India).

References

[1] Beck D D and Siegel R W 1992 *J. Mater. Res.* **7** 2840
[2] Richtsmeiser S C, Parks E K, Liu K, Pobo L G and Riley S J 1985 *J. Phys. Chem.* **82** 3659
[3] Wang Y and Mahler W 1987 *Opt. Commun.* **61** 233
[4] Banyai L, Hu Y Z, Lindberg M and Koch S W 1992 *Phys. Rev.* B **38** 8142
[5] Ricard D, Roussignol P, Hache F and Flytzanis C 1990 *Phys. Status Solidi* b **159** 275
[6] Alfassi Z, Bahnemann D and Henglein A 1982 *J. Phys. Chem.* **86** 4656
[7] Haase M, Weller H and Henglein A 1988 *J. Phys. Chem.* **92** 1103
[8] Goldstein A N, Echer C M and Alivisatos A P 1992 *Science* **256** 1425
[9] Potter B G Jr and Simmons J H 1988 *Phys. Rev.* B **37** 10 838
[10] Tanahashi I, Tsujimura A, Mitsuyu T and Nishino A 1990 *Japan. J. Appl. Phys.* **29** 2111
[11] Nesheva D and Levi Z 1997 *Semicond. Sci. Technol.* **12** 1319
[12] Lefebvre P, Mathieu H, Allegre J, Richard T, Combettes-Roos A, Pauthe M and Granier W 1997 *Semicond. Sci. Technol.* **12** 958
[13] Tsunetomo K, Nasu H, Katiyama H, Kawabuchi A, Osaka Y and Takiyama K 1989 *Japan. J. Appl. Phys.* **28** 1928
[14] Nasu H, Tsunetomo K, Tokumitsu Y and Osaka Y 1989 *Japan. J. Appl. Phys.* **28** L862
[15] Ochoa O R, Colajacomo C, Witkowski E J III, Simmons J H and Potter B G Jr 1996 *Solid State Commun.* **98** 717
[16] Potter B G Jr and Simmons J H 1990 *J. Appl. Phys.* **68** 1218
[17] Rajh T, Micic O I and Nozik A J 1993 *J. Phys. Chem.* **97** 11 999
[18] Suzuoki Y, Matsuno N, Tabata A, Takeda M and Mizutani T 1995 *Japan. J. Appl. Phys.* **34** 1631
[19] *Handbook of Chemistry and Physics* 70th edn 1989–90 (Boca Raton, FL: CRC Press)
[20] Berming P H 1967 *Phys. Thin Films* **1** 69
[21] Bennett H E and Bennett J M 1967 *Phys. Thin Films* **4** 1
[22] Donovan T M, Spicer W E, Bennett J M and Ashley E J 1970 *Phys. Rev.* B **2** 397
[23] Tauc J 1970 *Optical Properties of Solids* ed F Abeles (Amsterdam: North-Holland)

[24] Angel O Z, Alvaratos Gul J J, Lozada-Maorales R, Vargas H and de Silva A F 1994 *Appl. Phys. Lett.* **64** 291
[25] Ramirez-Bon R, Espinoza-Beltran F J, Arizpe-Chavez H, Zelaya-Angel O and Sanchez-Sinencio F J 1995 *Appl. Phys.* **77** 5461
[26] Efros Al L and Efros A L 1982 *Sov. Phys.–Semicond.* **16** 772
[27] Willardson R K and Beer A C (ed) 1978 *Semiconductor and Semimetals, Cadmium Telluride* vol 13 (New York: Academic)
[28] Minoru Fujii, Osamu Mamezaki, Shinji Hayashi and Keiichi Yamamoto 1998 *J. Appl. Phys.* **83** 1507
[29] Simanek E 1981 *Solid State Commun.* **40** 1021
[30] Hohl G F, Baranovskii S D, Beckerv, Hensel F, Quaiser S A and Reetz M T 1995 *J. Appl. Phys.* **78** 7130
[31] Lampart M M and Mark P (ed) 1970 *Current Injection in Solids* (New York: Academic) chapters 4 and 8